REPORT

GEOPHYSICS

Optical polarization–based seismic and water wave sensing on transoceanic cables

Zhongwen Zhan[1]*, Mattia Cantono[2], Valey Kamalov[2], Antonio Mecozzi[3], Rafael Müller[2], Shuang Yin[2], Jorge C. Castellanos[1]

Seafloor geophysical instrumentation is challenging to deploy and maintain but critical for studying submarine earthquakes and Earth's interior. Emerging fiber-optic sensing technologies that can leverage submarine telecommunication cables present an opportunity to fill the data gap. We successfully sensed seismic and water waves over a 10,000-kilometer-long submarine cable connecting Los Angeles, California, and Valparaiso, Chile, by monitoring the polarization of regular optical telecommunication channels. We detected multiple moderate-to-large earthquakes along the cable in the 10-millihertz to 5-hertz band. We also recorded pressure signals from ocean swells in the primary microseism band, implying the potential for tsunami sensing. Our method, because it does not require specialized equipment, laser sources, or dedicated fibers, is highly scalable for converting global submarine cables into continuous real-time earthquake and tsunami observatories.

The oceans present a major gap in geophysical instrumentation, hindering fundamental research on submarine earthquakes and Earth's interior structure as well as effective earthquake and tsunami warning for offshore events. The data gap motivates many technologies, such as ocean-bottom seismic or pressure sensors, cabled geophysical observatories (*1*), autonomous vehicles (*2*), and floats with hydrophones (*3*). Emerging fiber-optic sensing technologies bring a different possible solution. Marra *et al.* turned a 96-km-long submarine cable into a sensitive seismic sensor using ultrastable laser interferometry of a round-trip signal (*4*). Another technology, distributed acoustic sensing (DAS), interrogates intrinsic Rayleigh backscattering and converts tens of kilometers of dedicated fiber into thousands of seismic strainmeters on the seafloor (*5*–*7*). If a fraction of the million-kilometer submarine fiber-optic network could function as geophysical sensors, we would have a large increase in data coverage for large portions of the seafloor. Sites of interest for geophysical interrogation, such as the Hawaii or Iceland hotspots, and coastal cities next to subduction zones are often key nodes in telecommunication networks. The abundant number of fibers around them, if mobilized for geophysical research, could provide critical data for assessing geohazards and investigating seafloor and ocean processes.

Major obstacles exist on the path toward global fiber-based geophysical networks on the seafloor. Unlike their counterparts on land, submarine cables are extraordinarily expensive to deploy, heavily used, and strictly regulated. As the backbone of global internet connectivity, long-haul submarine cables usually have surprisingly few fiber strands (~2 to 6 pairs). Therefore, unused strands of fiber (called dark fibers), which are currently required for DAS, are rare. Furthermore, to take full advantage of long transoceanic cables, DAS needs to both function across frequent repeaters and drastically increase its range (which is currently ~50 km) (*8*). Techniques that rely on sophisticated and expensive equipment, such as ultrastable laser sources (*4*) or repeaters with built-in geophysical sensors required specifically for geophysical sensing (*9*), raise cost and security concerns depending on the extent of equipment changes needed, sensitivity of collected information, and data policies. Additionally, the installation of sensing equipment in facilities where telecommunications equipment sits can raise security concerns with regard to eavesdropping and service disruption. These practical considerations make

[1]Seismological Laboratory, Division of Geological and Planetary Sciences, California Institute of Technology, Pasadena, CA, USA. [2]Google LLC, Mountain View, CA, USA. [3]Department of Physical and Chemical Sciences, University of L'Aquila, Coppito, Italy.
*Corresponding author. Email: zwzhan@caltech.edu

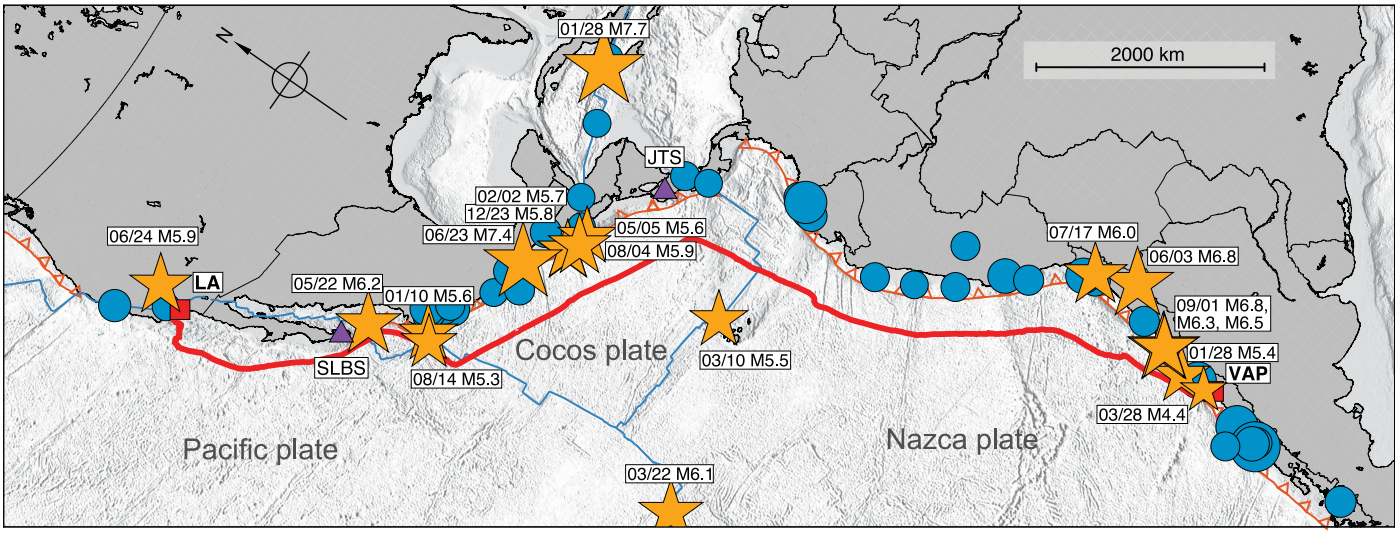

Fig. 1. Tectonics and earthquakes along the Curie cable. The Curie cable (red curve) is a 10,000-km-long submarine fiber-optic cable connecting Los Angeles (LA) and Valparaiso (VAP) along or across a series of active plate boundaries (blue and orange barbed lines). More than 50 earthquakes with a magnitude of >7.5 (blue dots) have occurred in this region since 1900. During our initial test period of SOP sensing (December 2019 to September 2020), we detected ~20 moderate-to-large earthquakes (yellow stars labeled with date and earthquake magnitude), most of which occurred in the Central and South American subduction zones. JTS and SLBS (purple triangles) are coastal seismic stations along the Curie cable.

large-scale incorporation into existing or future submarine cables challenging.

We took a different approach and turned the 10,000-km submarine cable "Curie" into a geophysical instrument that detected both earthquake shaking and ocean waves. The Curie cable was deployed in 2019 by Google to connect Los Angeles, California, and Valparaiso, Chile, along the eastern edge of the Pacific Ocean (Fig. 1 and fig. S1) (*10*). From north to south, the cable crosses multiple faults offshore of southern California and then crosses the Eastern Pacific Rise three times onto the Cocos Plate. Most of the length of the cable lies along the Central American and South American subduction zones at ~400 km to the ocean side of the trenches. Along the open-ocean cable section, the water depth is 4000 m on average but can be as shallow as 2000 m near the oceanic ridges and plateau and as deep as 6000 m when crossing the trench near Valparaiso. Near this path, more than 50 shallow earthquakes with a moment magnitude (M_w) larger than 7.5 have occurred since 1900 (Fig. 1, blue dots), 10 of which were larger than M_w8.0 and posed a substantial threat of shaking and tsunami. Two events are particularly notable: The 1960 Chilean M_w9.5 earthquake is the largest ever recorded (*11*), and the 1985 Mexico City M_w8.0 earthquake devastated the city (*12*).

We monitored the state of polarization (SOP) of regular optical telecommunication traffic through the Curie cable (fig. S2). The SOP can be represented by the Stokes parameters and visualized on the Poincaré sphere (*13*) (Fig. 2A). Whereas the SOP of the transmit laser is stable over a long time scale (e.g., days), the output SOP at the receiver end is, in general, different from the input SOP and changes over time owing to various external perturbations to the fiber (*10*, *14*, *15*). For terrestrial fibers, the output SOP can be chaotic and hard to interpret owing to substantial temperature variations along cable and air flow or human-, animal-, and/or traffic-induced vibrations when integrated over the entire optical path. Extreme SOP transients with up to 5 Mrad/s anomalies were observed during lightning strikes (*16*). However, by making orders-of-magnitude more sensitive measurements, we found the output SOP of the Curie transcontinental submarine cables to be much more stable compared with that of terrestrial cables, because the absolute majority of the path is in the deep ocean with almost constant temperature and minimal mechanical or electromagnetic perturbations (Fig. 2B). Therefore, strong seismic waves or long-period water waves produced by earthquakes close to the Curie cable can cause distinct and observable SOP anomalies (Fig. 2C).

In modern fiber-optic systems, polarization multiplexing is widely used to enhance the data transmission rate (*17*). The signal SOP is routinely recovered at the receivers to avoid cross-talk and ensure correct reception of the transmitted signals (*18*). This operation is performed by an adaptive digital equalizer implemented in application-specific integrated circuits (ASICs) (*19*, *20*). By accessing the internal registers of the ASICs, we measured SOP at sampling rates of tens of hertz on the vast majority of commercially available optical coherent transponders (*10*). Therefore, our approach adds minimal burden to the installation and operation of the submarine cable systems.

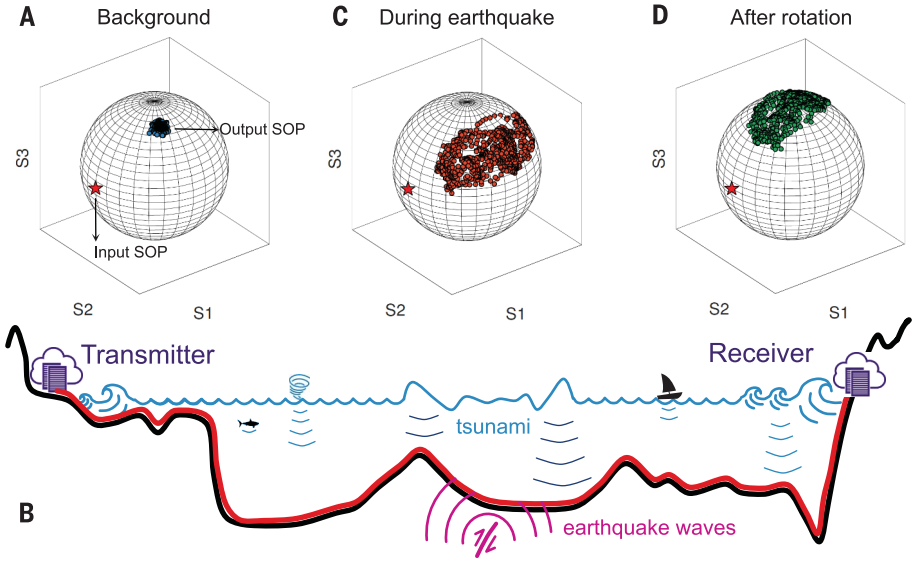

Fig. 2. Principles of polarization-based geophysical sensing. (**A**) The state of polarization (SOP) at the receiver is monitored routinely (blue dots on the Poincaré sphere) while the input SOP stays stable (red star). For the Curie cable, the output SOP is robust, owing to relatively minimal perturbations along most of its path in the deep ocean (**B**). The robustness allows us to detect earthquakes or ocean waves that produce SOP anomalies by shaking or pressuring the cable (**C**). Because the three Stokes parameters are normalized to 1.0, only two are independent. In this study, we rotate the Stokes parameters to the north pole of the Poincaré sphere (*9*) and focus on analyzing the S1 and S2 parameters after rotation (**D**).

Because two of the three Stokes parameters are independent given the unit length of the normalized polarization vector, we rotated the SOP measurements toward the north pole on the Poincaré sphere over a 200-s moving-window average (*10*). Effectively working as a high-pass filter, the rotation operation also helped reduce the effect of long-term SOP drifts of unknown origin in our experimental setup, potentially owing to temperature variations and mechanical vibrations over the short land sections of cable at both ends. After rotation (Fig. 2D), S1 and S2 of the Stokes parameters had values centered around zero, allowing a more straightforward spectral analysis.

During our test period from 15 December 2019 to 4 September 2020, the largest subduction zone event along the Curie cable was the 23 June Oaxaca, Mexico, magnitude 7.4 (*M*7.4) earthquake. The event was ~500 km to the cable at the closest point (Fig. 1). The strong SOP perturbations caused by the shaking lasted more than 20 min (Fig. 3, A and B). In comparison, the vertical-component shaking recorded at the UNM (National Autonomous University of Mexico) seismic station in Mexico City, also ~500 km from the earthquake, lasted ~5 min. The signal durations differ because the SOP measurements reflect the integrated effects of shaking along thousands of kilometers of cable over which the light polarization is perturbed.

The integral effect of SOP along the cable complicates our picking of the primary and secondary (*P* and *S*) waves, especially for large events, such as the Oaxaca M_w7.4 earthquake, that also have long rupture durations. On 3 June 2020, we detected on SOP a M_w6.8 intermediate-depth earthquake underneath Peru, 200 km landward of the coast and 680 km from the Curie cable. Because of the longer distance and the short source durations of intermediate-depth earthquakes (*21*), we were able to identify clearly separated *P* and *S* wave packages in the 0.8 to 3 Hz frequency band (Fig. 3, D and F). Somewhat unexpectedly, 350 s after the earthquake origin time, another package of strong but lower-frequency (0.3 to 0.8 Hz) waves arrived at the Curie cable (Fig. 3, E and F). Given the waves' slow average speed (~2 km/s) and the non-excitation of short-period surface waves from the earthquake at 97 km depth (see fig. S4 for an example of surface waves on SOP), we believe that these late waves are either ocean acoustic

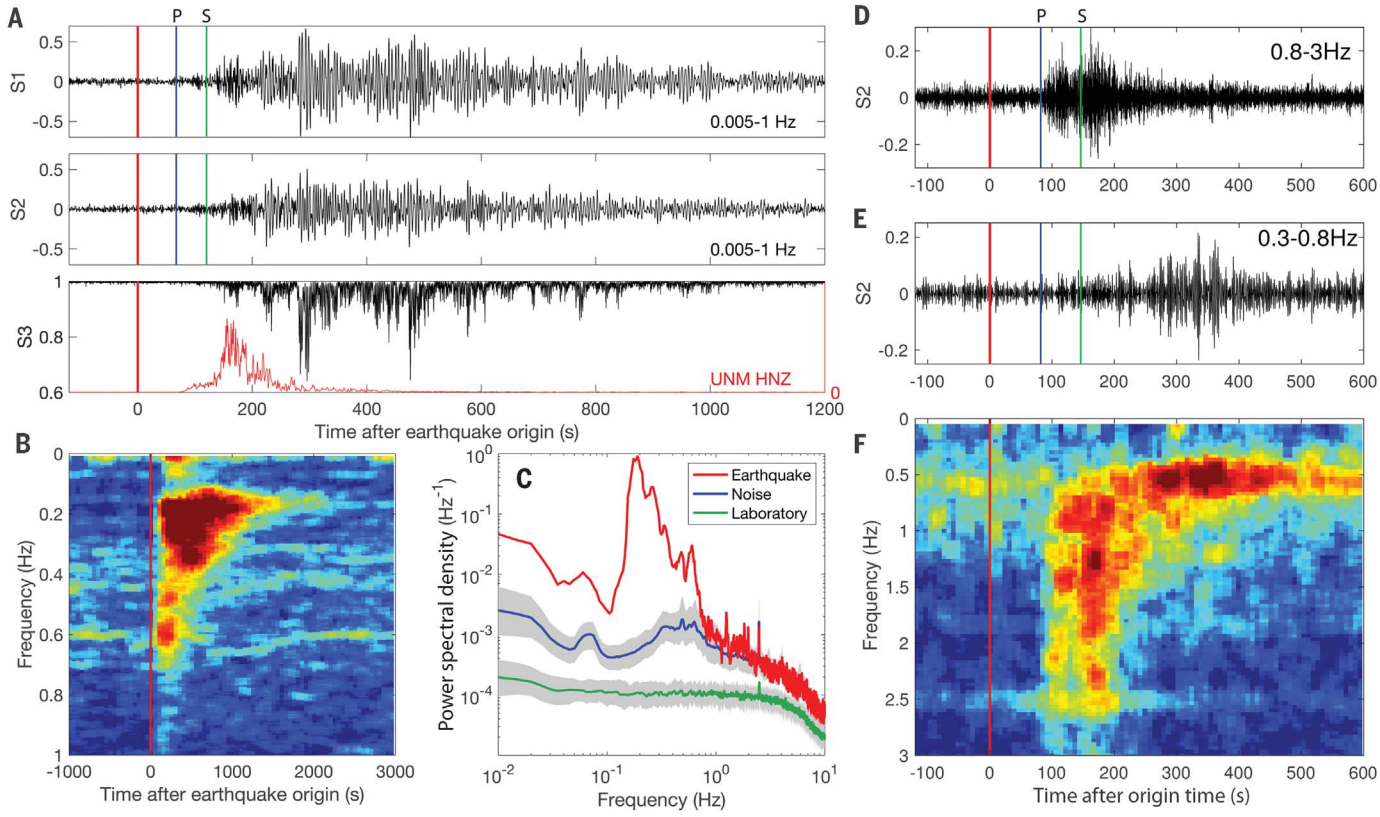

Fig. 3. Earthquake detections along the Curie cable. (**A**) The Curie SOP anomaly from the 23 June 2020 Oaxaca *M*7.4 earthquake (Fig. 1) lasted more than 20 min, substantially longer than the shaking duration at the UNM station in Mexico City (seismic envelope shown in red). (**B**) The summed spectrogram for S1 and S2 show broadband signals from 0.01 to 1 Hz, with a strong and prolonged amplification between 0.15 and 0.35 Hz, as confirmed by the power spectral density (PSD) in the first 5 min of the SOP anomaly [red curve in (C)]. The blue curve and gray band in (**C**) represent the median noise PSD on the same day and the 1σ confidence interval, respectively. The PSD peak at ~0.06 Hz corresponds to ocean swells. The instrumental noise measured in the laboratory environment is shown as the green curve. (**D** to **F**) For a more impulsive M_w6.8 intermediate-depth earthquake on 3 June 2020, we observed distinct *P* and *S* wave packages on SOP between 0.8 and 3 Hz [(D) and (F)], and potentially ocean acoustic waves or Scholte waves at slightly lower frequencies [(E) and (F)]. The vertical red lines in all panels mark the earthquake origin time. The vertical blue and green lines in (A), (D), and (E) are theoretical earthquake *P* and *S* wave arrival times, respectively, to the closest point along the cable.

waves or Scholte waves converted from the direct *P* and *S* waves near bathymetric features (e.g., slopes, trench) (*22*, *23*) and subseafloor heterogeneities (e.g., fault zones) (*7*). The same mechanism must have contributed to the long SOP signal durations for shallow earthquakes close to the trenches (e.g., Fig. 3A), in addition to the intrinsic integral effect of SOP measurements, as discussed earlier.

For tsunami warning, a key application of seafloor geophysics, the ability to detect water waves is critical for confirming, adjusting, or lifting the initial warnings on the basis of the faster seismic waves (*24*). This process is currently achieved by a sparse network of ~60 DART (Deep-ocean Assessment and Reporting of Tsunamis) buoys around the globe, mostly along subduction zones. The high cost of installing and maintaining DARTs limits sensor density. If tsunami waves could instead be detected along submarine cables, the broader data coverage, higher sampling rate, and faster telemetry could supplement current DART systems to provide faster and more reliable tsunami warnings (*25*). During our test period, only the Oaxaca M_w7.4 earthquake produced tsunami waves (~1 cm high in the open ocean), which were not detected by our current SOP measurement system. In this prototype, the SOP noise is higher at long periods where we expect the tsunami waves (fig. S5), potentially because of temperature variations over the 7.7-km land section of cable (*10*). In a well-controlled laboratory environment, the SOP noise level is substantially lower than the field observations over a broad frequency band, between 0.01 and 10 Hz (Fig. 3C).

However, in the primary microseism frequency band (~0.06 Hz), we observed multiple packages of dispersive signals from ocean swells, each of which lasted for a few days (Fig. 4A). The timing of the wave packages coincides well with the primary and secondary microseism pairs observed at coastal seismic stations located along the cable, as shown in Fig. 4, B and C, for two representative stations, SLBS (Sierra la Laguna Baja California Sur, Mexico) and JTS (Las Juntas de Abangares, Costa Rica) (station location shown in Fig. 1). Microseism signals at coastal sites are related to ocean swells produced by distant storms (*26*). In particular, the double-frequency secondary microseism (i.e., the seismic waves produced by wave-wave interactions) was not observed on SOP. Therefore, we suggest that the dispersive wave packages on SOP are caused by seafloor pressure perturbations from ocean swells in shallow water, not by the passing seismic waves on the seafloor. The amplitudes of ocean swells are comparable to those of damaging tsunami waves observed in the open ocean (e.g., on the order of 1 m for the 2004 Sumatra and 2011 Tohoku earthquakes) (*27*, *28*). Given the much longer period of tsunami waves and therefore negligible decay as a function of depth, the seafloor pressure signal of a tsunami in the open ocean would be comparable or stronger for detection on SOP than that of ocean swells. The SOP detection of tsunami waves in

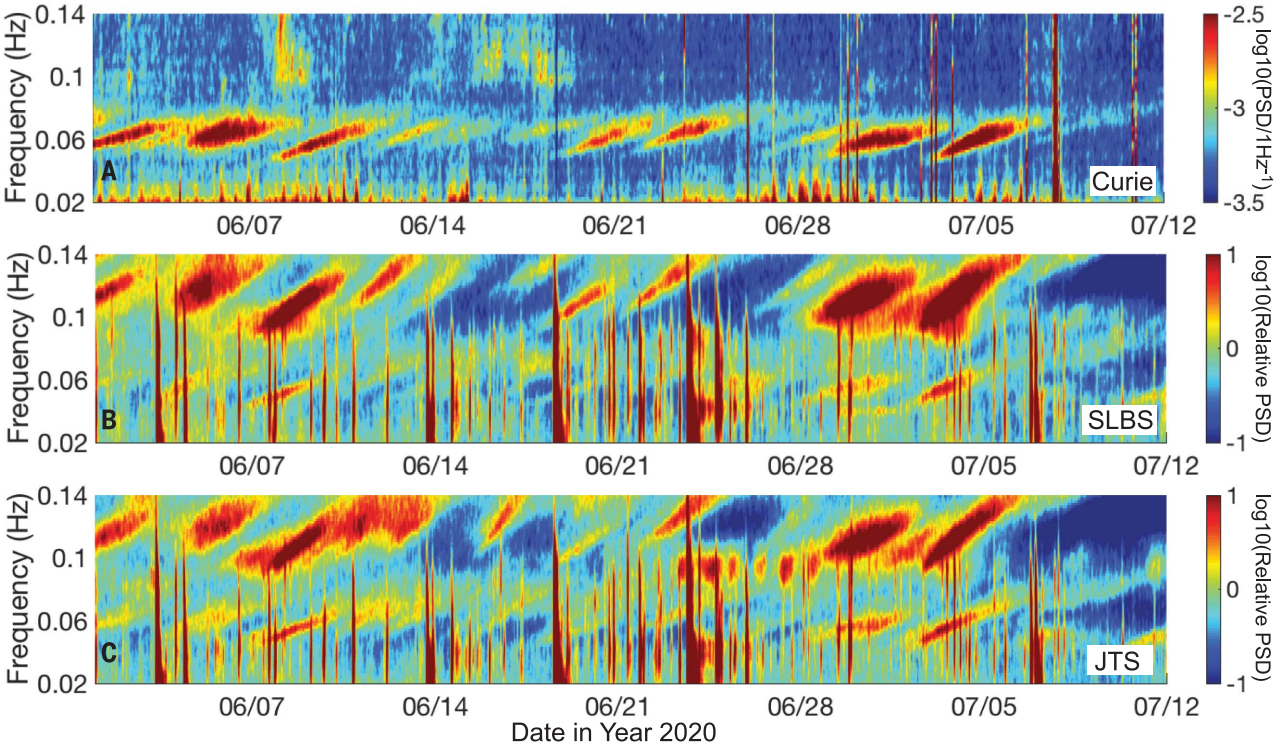

Fig. 4. SOP detection of ocean swells. (**A**) SOP spectrogram from 1 June 2020 to 12 July 2020. The dispersive energy packages around 0.06 Hz, in the primary microseism band, correlate well with similarly dispersive events on the relative spectrograms of coastal station (**B**) SLBS and (**C**) JTS (with mean PSD removed; station locations shown in Fig. 1), in the primary and secondary (~0.12 Hz) microseism bands. The amplitudes of the SOP events and the microseism events are consistent overall too, which is confirmed more quantitatively in fig. S6.

the open ocean is critical for effective tsunami warning.

For estimating earthquake magnitudes and forecasting tsunami wave heights, accurate SOP amplitudes of the recorded seismic and water waves are critical. Without colocated ocean-bottom seismometers or pressure sensors of similar sampling rates, calibrating the SOP amplitudes in a broad frequency band is challenging. However, we found that the amplitudes of the ocean swell events on SOP (Fig. 4A) correlate well with the strengths of the secondary microseism events at coastal seismic stations (Fig. 4, B and C) for ~30 distant storms throughout the testing period (fig. S6). Correlations may exist for the primary microseisms as well, but the data are noisy. These observations suggest that the SOP amplitude scaling has been linear and robust at least around 0.06 Hz over the 9-month observation period.

For the seismic waves, the SOP amplitude response is broadband but not flat. For example, the S1 and S2 polarization signals of the Oaxaca M_w7.4 earthquake are above the noise level between 0.01 and 1 Hz, but with the strongest peak and prolonged signals between 0.15 and 0.35 Hz (Fig. 3, B and C). The SOP earthquake signals were consistently stronger or only visible in the 0.15- to 0.35-Hz band for the nine events detected along the Central American cable section (Fig. 1), which allows us to explore amplitude scaling there. We found that the earthquakes' average SOP power spectral densities in the 0.15- to 0.35-Hz band showed an overall positive correlation with the predicted peak ground displacement in the same band, but with still unclear quantitative relations (fig. S7). We observed even more broadband SOP signals from 0.01 to 5 Hz for the 1 September M_w6.8 earthquake offshore of Vallenar, Chile (figs. S8 and S9), but with the strongest energy between 0.3 and 1.5 Hz instead. Given the consistent components (e.g., cable, repeaters) and installation method along the Curie cable, the differences in the frequency peaks between the Mexico and Chile sections may indicate effects from water depths and site conditions. However, the consistent low-frequency sensitivity around 0.01 Hz is critical to estimating the moment magnitudes of large tsunamigenic earthquakes (*29*). Determining the dynamic range of SOP measurements and whether the cable-seafloor coupling plays an important role requires further observations.

Like the ultrastable laser interferometry approach (*4*), the SOP-based sensing integrates the mechanical perturbations over the entire optical path to produce a single SOP time series per channel. The source locations cannot be uniquely determined from a single channel. However, because the SOP approach is highly scalable with minimal modifications to existing cable systems, we expect to be able to use multiple lit cables with different paths in a given region. Once the SOP timings of the different cables are synchronized (*10*), their seismic travel times could be combined to locate sources (*4*). For tsunami warning, the current seismic systems usually produce adequate origin times and locations promptly (*25*). The SOP measurements could then be jointly interpreted with the seismic and DART data to constrain earthquake magnitudes and refine tsunami forecasts. Furthermore, a suite of geophysical sensing techniques based on submarine telecommunication cables are emerging, with different levels of sensitivity, coverage, spatial resolution, and scalability (*4*–*9*). Strategic combinations of the different sensing techniques (including conventional geophysical networks) are necessary to provide the broadest coverage of the seafloor while making high-fidelity, physically interpretable measurements (e.g., locations, depth, and magnitudes).

To our knowledge, our experiment is the first direct demonstration that transcontinental submarine cables can be used for

environmental monitoring through sensing capabilities, in particular earthquake and ocean wave detections. The coherent subsea cable SOP detection technique showed the sensitivity level of an optical polarization interferometer (*30*). We find it remarkable that by monitoring the SOP of regular optical telecommunication channels via routine equipment, we detected vibrations with peak displacement as small as 0.1 mm (fig. S7) over a 10,000-km submarine cable, or 20,000 km in the round-trip channels (Fig. 1 and fig. S2). The fraction of a wavelength change in the optical path of two orthogonal polarizations implies a high relative phase to polarization stability resulting in relative optical path variation better than 10^{-14}. Substantial room exists to improve the SOP system. For example, the number of SOP channels in a single undersea cable can be the same as the number of telecommunication channels, on the order of hundreds with multiple frequencies per fiber strand (fig. S2). We expect to improve the SOP signal-to-noise ratio by combining these independent SOP measurements from multiple transponders operating on the same cable (fig. S10). Reduction of SOP noise level at high frequencies (1 to 10 Hz) would allow detection of small earthquakes that might not be detectable on terrestrial seismic networks far away, and at low frequencies (<0.01 Hz) would enable accurate magnitude estimation for large earthquakes and direct observation of tsunami waves. With appropriate timing mechanisms (*10*), the SOP system would be able to sense strong seismic or ocean waves anywhere along a 10,000-km path within 30 ms of the first wave arrivals at a submarine cable, substantially faster than the closest land-based stations in many cases (e.g., fig. S11).

REFERENCES AND NOTES

1. D. Suetsugu, H. Shiobara, *Annu. Rev. Earth Planet. Sci.* **42**, 27–43 (2014).
2. R. Bürgmann, D. Chadwell, *Annu. Rev. Earth Planet. Sci.* **42**, 509–534 (2014).
3. G. Nolet *et al.*, *Sci. Rep.* **9**, 1326 (2019).
4. G. Marra *et al.*, *Science* **361**, 486–490 (2018).
5. E. F. Williams *et al.*, *Nat. Commun.* **10**, 5778 (2019).
6. A. Sladen *et al.*, *Nat. Commun.* **10**, 5777 (2019).
7. N. J. Lindsey, T. C. Dawe, J. B. Ajo-Franklin, *Science* **366**, 1103–1107 (2019).
8. Z. Zhan, *Seismol. Res. Lett.* **91**, 1–15 (2020).
9. B. M. Howe *et al.*, *Front. Mar. Sci.* **6**, 424 (2019).
10. Materials and methods are available as supplementary materials.
11. H. Kanamori, L. Rivera, S. Lambotte, *Geophys. J. Int.* **218**, 1–32 (2019).
12. H. Eissler, L. Astiz, H. Kanamori, *Geophys. Res. Lett.* **13**, 569–572 (1986).
13. M. Born, E. Wolf, *Principles of Optics: Electromagnetic Theory of Propagation, Interference and Diffraction of Light* (Elsevier, 2013).
14. J. Wuttke, P. M. Krummrich, J. Rösch, *IEEE Photonics Technol. Lett.* **15**, 882–884 (2003).
15. P. M. Krummrich, E.-D. Schmidt, W. Weiershausen, A. Mattheus, "Field trial results on statistics of fast polarization changes in long haul WDM transmission systems," *Optical Fiber Communication Conference and Exposition and The National Fiber Optic Engineers Conference Technical Digest* (paper OThT6, Optical Society of America, 2005).
16. D. Charlton *et al.*, *Opt. Express* **25**, 9689–9696 (2017).
17. S. G. Evangelides, L. F. Mollenauer, J. P. Gordon, N. S. Bergano, *J. Lightwave Technol.* **10**, 28–35 (1992).
18. S. J. Savory, *IEEE J. Sel. Top. Quantum Electron.* **16**, 1164–1179 (2010).
19. G. Charlet *et al.*, *J. Lightwave Technol.* **27**, 153–157 (2009).
20. C. R. S. Fludger *et al.*, *J. Lightwave Technol.* **26**, 64–72 (2008).
21. M. Vallée, *Nat. Commun.* **4**, 2606 (2013).
22. E. A. Okal, *Adv. Geophys.* **49**, 1–65 (2008).
23. Y. Zheng, X. Fang, J. Liu, M. C. Fehler, arXiv:1306.4383 [physics.geo-ph] (18 June 2013).
24. E. Bernard, V. Titov, *Philos. Trans. R. Soc. London Ser. A.* **373**, 20140371 (2015).
25. National Research Council, *Tsunami Warning and Preparedness: An Assessment of the U.S. Tsunami Program and the Nation's Preparedness Efforts* (National Academies Press, 2011).
26. R. A. Haubrich, W. H. Munk, F. E. Snodgrass, *Bull. Seismol. Soc. Am.* **53**, 27–37 (1963).
27. V. Titov, A. B. Rabinovich, H. O. Mofjeld, R. E. Thomson, F. I. González, *Science* **309**, 2045–2048 (2005).
28. M. Simons *et al.*, *Science* **332**, 1421–1425 (2011).
29. H. Kanamori, L. Rivera, *Geophys. J. Int.* **175**, 222–238 (2008).
30. P. Grangier, R. E. Slusher, B. Yurke, A. LaPorta, *Phys. Rev. Lett.* **59**, 2153–2156 (1987).
31. Z. Zhan, Curie Data - Zhan *et al.*, Version 1.0, CaltechDATA (2021); https://doi.org/10.22002/D1.1668.

ACKNOWLEDGMENTS

We thank U. Holzle for initiating the subsea-based earthquake detection project. We thank B. Koley, V. Vusirikala, M. Salsi, M. Newland, T. Carlson, L. Bickford, S. Bhattacharya (Google LLC), M. Pan, J. Geyer (Acacia Inc.), S. Thodupunoori (Cisco Inc.), F. Santillo (Ciena Inc.), and Y. Svirko (University of Eastern Finland) for support and discussions. Earthquake information used in this study is from the U.S. Geological Survey. **Funding:** Z.Z. and J.C.C. are funded by the Gordon and Betty Moore Foundation. A.M. is partially funded by the Italian Government through the INCIPICT project. **Author contributions:** Z.Z., M.C., and V.K. designed the work. M.C., V.K., and S.Y. collected the SOP data. A.M., V.K., R.M., M.C., and S.Y. conducted the analyses in optics. Z.Z., J.C., and A.M. led the work on earthquakes and ocean waves. All authors participated in the data interpretation. Z.Z., A.M., M.C., R.M., V.K., and S.Y. prepared the initial draft, and all authors critically revised and approved the manuscript. **Competing interests:** A U.S. patent has been filed related to this work. **Data and materials availability:** SOP data used in this study are openly available on https://data.caltech.edu/records/1668 (*31*). More information about reading and processing the data files can be obtained from the authors upon request. Seismic data at the conventional stations are from the International Federation of Digital Seismograph Networks and the Global Seismic Network and downloaded through the Incorporated Research Institutions for Seismology.

SUPPLEMENTARY MATERIALS

science.sciencemag.org/content/371/6532/931/suppl/DC1
Supplementary Text
Figs. S1 to S12
References (*32*–*47*)

13 September 2020; accepted 11 January 2021
10.1126/science.abe6648

Science

Optical polarization–based seismic and water wave sensing on transoceanic cables

Zhongwen Zhan, Mattia Cantono, Valey Kamalov, Antonio Mecozzi, Rafael Müller, Shuang Yin and Jorge C. Castellanos

Science **371** (6532), 931-936.
DOI: 10.1126/science.abe6648

Waiting for earthquakes to call

Instrumenting the vast ocean floor is difficult and expensive but important for monitoring earthquakes and tsunamis. Zhan *et al.* used the polarization of regular telecommunication traffic to detect earthquakes and water swells in a 10,000-kilometer-long fiber-optic submarine cable (see the Perspective by Wilcock). The deep-water Curie cable is not as noisy as terrestrial counterparts, allowing the authors to detect strain from the cable. Results from the 9-month observation period showed how current submarine fiber-optic cables can also be used as a geophysical tool.

Science, this issue p. 931; see also p. 882

Science (print ISSN 0036-8075; online ISSN 1095-9203) is published by the American Association for the Advancement of Science, 1200 New York Avenue NW, Washington, DC 20005. The title *Science* is a registered trademark of AAAS.